International Journal of Coal Geology 88 (2011) 55–66

Contents lists available at SciVerse ScienceDirect

International Journal of Coal Geology

journal homepage: www.elsevier.com/locate/ijcoalgeo

Petrographic and geochemical effects of sill intrusions on coal and their implications for gas outbursts in the Wolonghu Mine, Huaibei Coalfield, China

Jing-Yu Jiang, Yuan-Ping Cheng *, Lei Wang, Wei Li, Liang Wang

National Engineering Research Center for Coal & Gas Control, China University of Mining & Technology, Xuzhou 221008, China

ARTICLE INFO

Article history:
Received 3 June 2011
Received in revised form 19 August 2011
Accepted 19 August 2011
Available online 26 August 2011

Keywords:
Sill intrusions
Outburst
Trap effect
Vitrinite reflectance
Thermal aureoles
Huaibei Coalfield

ABSTRACT

Since the early 1980s, fifteen outbursts have occurred in the Huaibei Coalfield of China. These outbursts were reported to be associated with sills. To study the effect of sill intrusions on coal seam and their relationship to methane outbursts, eleven samples from the No. 10 coal seam were taken from the Wolonghu Mine at various distances from a diorite sill. Comparisons were made between unaltered and heat-affected coals using petrographic and chemical data, micropore characteristics, adsorption properties of coal, and gas outburst indexes from field. Approaching the intrusion, vitrinite reflectance levels increased from 2.74% to 5.03%, and the thermal aureole of the sill ~60 m (from the sill boundary to sample 9). Three zones along this gradient were identified as corresponding to (1) thermal evolution zone No. 1 (0–5 m from sill), (2) thermal evolution zone No. 2 (5–60 m from sill), and (3) unaltered zone. The methane adsorption capacity of coal samples in the thermal evolution zone No. 2 was generally higher than in the two other zones, and the unaltered zone higher than the thermal evolution zone No. 1. It is concluded that the contact-metamorphism decreased the adsorption capacity of coal and the thermal evolution of sill increased it. The trap effect of sill, combined with the mudstone and siltstone roof and floor of the No. 10 coal seam, provided a seal for the formation of a gas pocket. Abnormally high formation pressures at the No. 10 coal seam led to two outbursts.

1. Introduction

Coals influenced by igneous intrusions are relatively common and occur in many localities worldwide. There have been numerous studies of the effects of intrusions on coal seams (Clegg, 1955; Cooper et al., 2007; Dai et al., 2011; Dai and Ren, 2007; Dutcher et al., 1966; Golab et al., 2006; Gurba and Weber, 2001; Rimmer et al., 2009; Saghafi et al., 2008; Sarana and Kar, 2011; Schimmelmann et al., 2009; Valentim et al., 2011). Most research has focused on the chemical and physical properties of coal samples at different distances from dikes, though several studies have investigated coal samples above and below sills.

Igneous intrusions thermally and geochemically alter coal, often causing safety problems for coal mines (Golab, 2004). Intrusions on coal seams cause significant increases in vitrinite reflectance (R_o), and fixed carbon (FC) and decreases in moisture, volatile matter (VM), hydrogen and nitrogen content adjacent to the magmatic intrusion (Rimmer et al., 2009; Saghafi et al., 2008; Stewart et al., 2005). In the Gunnedah Basin, alteration zones are 0.8 to 1 times the thickness of the sill (Gurba and Weber, 2001). The thermal alteration does not increase until 20 m above the igneous sill. It is only at 4.23 m above the sill that both thermal indicators raise steeply (Pross et al., 2007). The effect of intrusive (dolerite dyke) is manifested up to a distance of 48 m (Sarana and Kar, 2011). However, the thermal aureoles of sill intrusions still require rigorous research.

Five methane outbursts have occurred in coal mines of South Africa associated with dikes and sills in the early 1990s (Anderson, 1995; Saghafi et al., 2008). The interaction of tectonics and volcanism was believed to have a great influence on the process of initiating and on the progress of CO_2 outbursts (Beamish and Crosdale, 1998; Faiz et al., 2007; Li et al., 2011). Coal and gas outbursts are a major problem for safe and efficient coal exploitation in the magmatic intruded Donets Basin (Sachsenhofer et al., 2011). However, few studies have been conducted on relation between methane outburst and sill intrusions.

Since the early 1980s, fifteen outburst events have occurred in several underground mines of China. The methane outbursts at the three affected mines in the Huaibei Coalfield, were mainly in the vicinity of sill intrusions. Eleven outbursts occurred in four coal seams (under a 120 m thick sill) of the Haizi Mine since 1984. In 1993 and 1996, two outbursts occurred in the Shitai Mine. The locations of outbursts were 30 m and 50 m respectively from the sill. In 2006 and 2008, two methane outbursts occurred in the No. 10 coal seam of the Wolonghu Mine. The locations of the outbursts were 8 m and 38 m from the sill boundary. In 2009, a large outburst occurred in the No. 10 coal seam of the Haizi Mine and caused one death.

* Corresponding author.
E-mail address: jingyu-jiang@hotmail.com (J.-Y. Jiang).

0166-5162/$ – see front matter.
doi:10.1016/j.coal.2011.08.007

The four outbursts in Shitai and Wolonghu Mine were at coal beds of the same coal seam at different distances from the sill. Although the intrusion of magma into coal seams has been extensively researched, the effect of sill intrusions on the petrology and chemistry of coal beds at the same coal seam and the relationship between sill intrusions and methane outbursts remain poorly understood. To improve the safety and well-being of miners in China, this paper investigates the thermal aureoles of sill intrusions on coal beds at the same seam. Unaltered and heat-affected coals were compared using petrographic and chemical data, micropore characteristics, adsorption and desorption properties of coal, gas pressure and content from the field.

2. Regional geology

The Huaibei Coalfield is located in northern Anhui Province in China. It is one of the country's major coalfields, with 23 active underground coal mines (Zheng et al., 2008). The Wolonghu Mine is located in the northwestern Huaibei Coalfield and covers 28 km^2 (Fig. 1). The main coal-bearing layer of Wolonghu Mine belongs to the Carboniferous–Permian system (Fig. 2). The No. 10 coal seam is the main mining layer in panels South No. 1, which is also the research area (Fig. 3).

The coal rank in the Huaibei Coalfield varies from high volatile bituminous A to anthracites A and was influenced by the Cretaceous Yanshanian magmatic metamorphism (Liu, et al., 2009). which can be divided into four stages. The first stage is diorite igneous rock controlled by the E–W fault zone, which runs along the North Suzhou Fault (NSF). This diorite rock (approximately 145 Ma) was the source of magma in the Wolonghu Mine (Han, 1990).

Magmatism was widespread in the Wolonghu Mine, and the Carboniferous–Permian coal seam was affected by igneous rock, as well. The strongest influence is seen at the No. 10 coal seam. The mineable area of the South No. 1 panel accounts for about 48%, the other part is non-mineable as the coal was swallowed by igneous (Fig. 3). The thickness of the diorite sill invading the roof of the No. 10 coal seam is uniform, with an average thickness of nearly 4 m (Zhang et al., 2005).

The southern part of the Wolonghu Mine adjoins the NSF, is one of main regional tectonics in Huaibei Coalfield (Jiang et al., 2010). The NSF, 240 km long and 4–6 km wide, is a concealed faulted zone composed of several E–W faults crossing the Huaibei Coalfield, formed in the late Paleozoic coal-forming period (Han, 1990). In the Yanshan Period (tectonic events occurring in China and East Asia from the late Jurassic to Early Cretaceous) (Yang et al., 2011), magma upwelled through the NSF, invading the Wolonghu Mine. The F_2 and F_7 faults controlled the direction and distribution of the intrusions (Figs. 1 and 3).

3. Sampling and methodology

To study the effect of sill intrusion on the properties of the coal, samples were obtained from the Wolonghu Mine of the Anhui Hengyuan

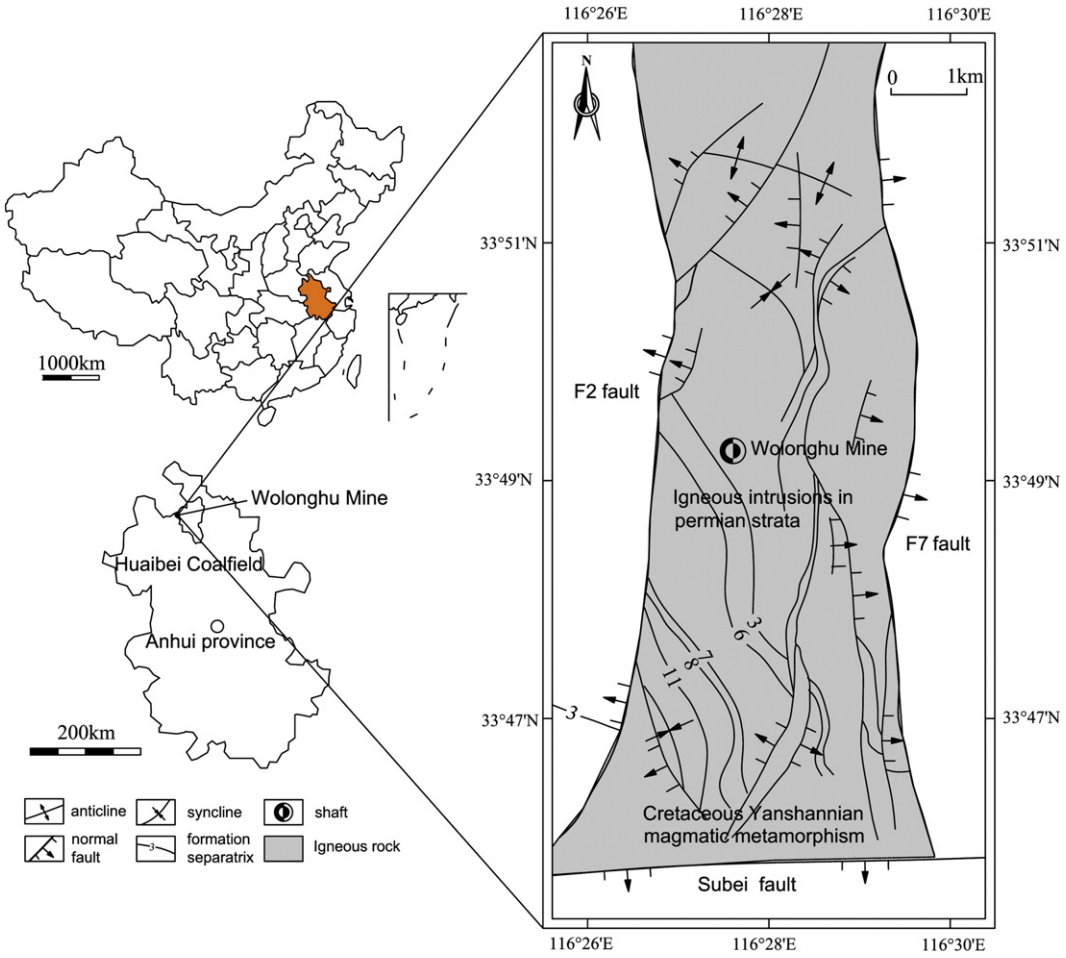

Fig. 1. Map showing study area and data locations for petrographic and geochemical characteristics of the coals from Wolonghu Mine.

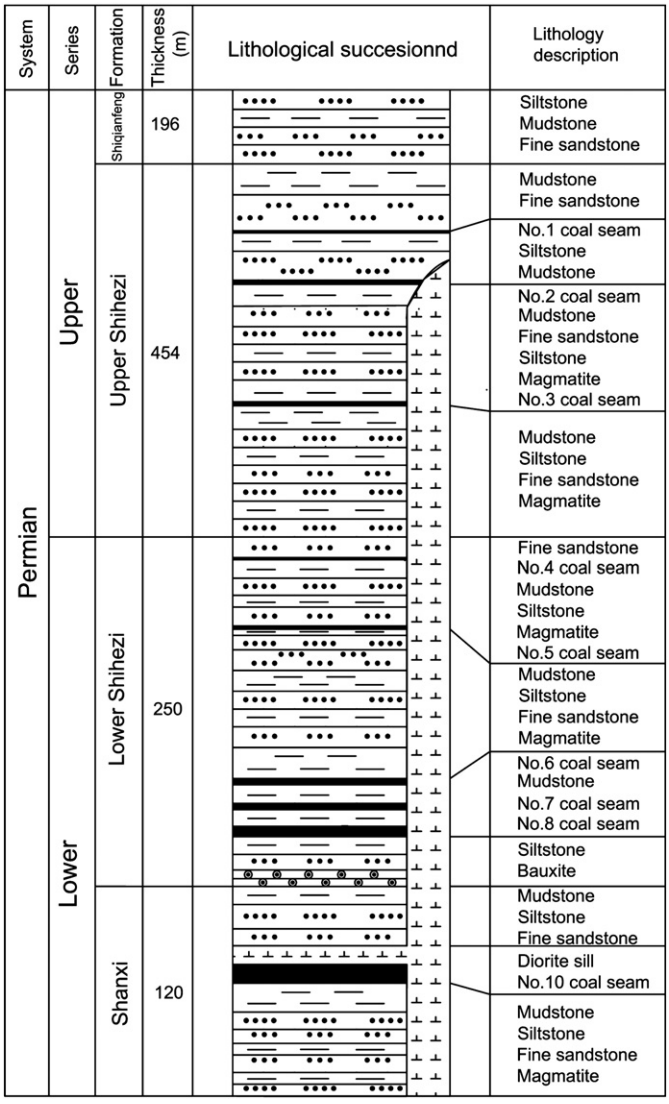

Fig. 2. Generalized stratigraphy of Wolonghu Mine.

Coal Co., Ltd. Eleven coal samples were collected along the roadway of coalface 102, at different distances from the sill (Figs. 3 and 4).

The proximate analysis was followed ASTM standards (ASTM, 2007). The ultimate analysis was according to the national standards of China GB/T 476–2008. Random vitrinite reflectance (R_o) measurements were performed using (Zeiss, Germany) microscope photometer, according to international standards (ISO 7404–5, 1984). The maceral composition of the coals was determined by incident light microscopy and oil immersion, according to international standards (Taylor et al., 1998). For the gas adsorption isotherm, crushed coal samples of 50 g and 0.2 to 0.25 mm particle size, exposed to gas pressures of up to ~5 MPa at 30 °C. A device (WT-I, Fushun Coal Science Research Institute, Liaoning, china) was used to measure initial gas-releasing rate, ΔP index according to standards (State Administration of Coal Mine Safety of China, 2009a). The gas adsorbed by crushed coal samples of 3.5 g of 0.2 to 0.25 mm particle size at a pressure of 0.1 MPa is released into fixed vacuum space. The pressure rise in the space for the period of 10–60 s after the release, ΔP (in mm Hg), is an index representing the gas emission capacity of the coal. The BET specific surface were obtained using nitrogen gas as the adsorptive at the boiling point temperature of liquid nitrogen (77.35 K at 101.3 kPa, SSA-4200, Beijing Builder Technology Co.LTD, china), whereas micropore volume, micropore surface area, and micropore size distribution were determined using low-pressure CO_2 at 273 K (AUTOSORB-1, Quantachrome Instruments Co., USA). Mean random vitrinite reflectance (R_o) can be converted to maximum paleo temperature attained (T_{peak}) using the relationship established by Barker and Pawlewicz (1994), providing an independent measure of the coal/sill contact temperature:

$$T_{peak} = (\ln(R_o) + 1.19)/0.00782 \quad (1)$$

In the field, underground gas pressure was measured following China's national standard (State Administration of Coal Mine Safety of China, 2007). The gas content was measured underground by the direct method provided in China's national standard (State Administration of Coal Mine Safety of China, 2008).

4. Results and discussion

4.1. Petrographic analyses

The vitrinite reflectance values, vitrinite, inertinite and subdivision of maceral composition of coal samples are listed in Tables 1 and 2. The R_o increases from 2.74% (as measured by oil immersion) to 5.03% directly contact to the sill. Samples 1–6 can be identified as anthracites A, samples 7 and 8 (anthracites B) and samples 9–11 belong to anthracites C. Unaltered coal sample 11 (95.1 m from the sill) has R_o of ~2.74%, coal sample 1 (0.2 m from the sill) adjacent to the intrusion has R_o of ~5.03% (Table 1). Temperatures of the Wolonghu coal can be estimated from Barker and Pawlewicz's (1994). The thermal evolution temperature (°C) of the Cretaceous Yanshanian magmatic metamorphism to the No. 10 coal seam is estimated to be at least 359 °C (Table 1).

Megascopic appearance of the sill igneous intrusion No. 10 coal seam is shown in (Fig. 5a). The diorite-type sill was mostly gray with some light brown sections. Sill/coal boundaries were irregular. Petrographically, the samples are high in vitrinite (Fig. 5b,d,h). For example, sample 11 ($R_o = 2.74\%$) contained 74.2% identifiable vitrinite (Table 1), and 70.1% of the heat-affected coal sample 2 ($R_o = 4.89\%$) was vitrinite. Vitrinite was dominated by collotelinite (Table 2). Inertinite (Fig. 5d,e,g) was dominated by fusinite and semifusinite (Table 2).

Coals close to the sill showed clear indications of thermal alteration expressed by the formation of devolatilization vacuoles and a fine mosaic texture of altered vitrinite (Fig. 5b,c). Clay in the form of veins or cell fillings was shown in (Fig. 5h). Framboidal pyrite enrichment was observed in coal sample 6 (Fig. 5f). Liptinite macerals were not found in the 11 coal samples (Fig. 5b–h) of anthracite rank with R_o between 2.74% and 5.03%. Liptinite fluorescence will lost when the R_o exceeds 1.3%, because it is already transformed in hydrocarbons due to the rank reached by these coals (Stach, et al., 1982; Taylor, et al., 1998).

The R_o curve shows a rapid increase from coal sample 9 (56.3 m from sill) to sample 1, 0.2 m from sill (Fig. 6a). The values of R_o from samples 11 to 9 are consistent, and we thus believe that samples 11 and 10 were not within the scope of the thermal aureoles. Thus the thermal aureoles of the sill intruding into the No. 10 coal seam are approximately 60 m (Figs. 4 and 6a). Based on the thermal aureoles divided by values of R_o, the sill intrusion area can be divided into three zones: (1) thermal evolution zone No. 1 (0–5 m from the sill), (2) thermal evolution zone No. 2 (5–60 m from the sill), and (3) unaltered zone. Thus, coal samples 1–5 (below the sill) belong to the thermal evolution zone No. 1, samples 6–9 are in the thermal evolution zone No. 2 and samples 10 and 11 are in the unaltered zone (Fig. 4).

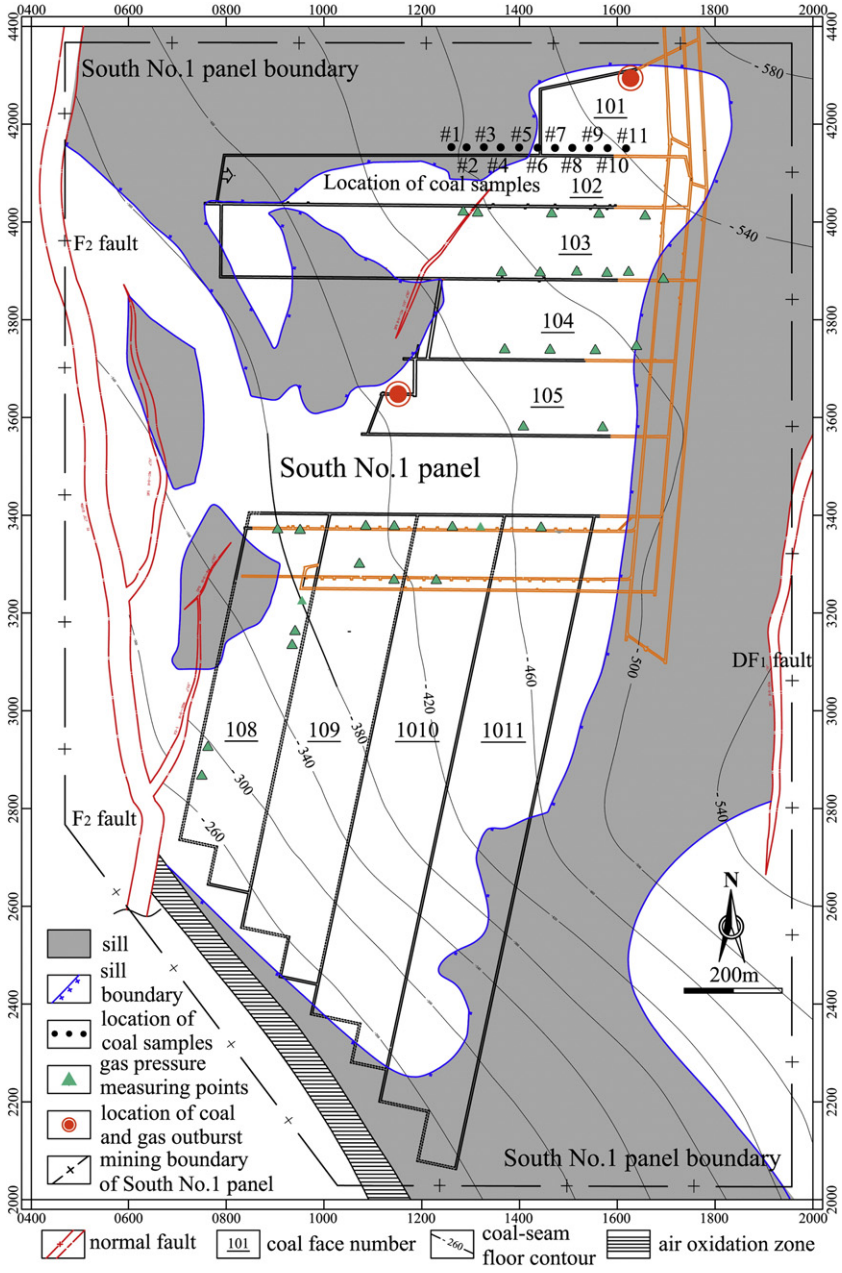

Fig. 3. Planar graph of igneous intrusions and coalfaces in South No. 1 panel of No. 10 coal seam.

4.2. Geochemical analyses

Moisture, ash, volatile matter, fixed carbon, and the C, H, O, N, and S elemental compositions of the coal samples are listed in Table 1. The intrusion affected coal composition (VM, ash, and moisture) beyond a distance of ~60 m. Whole-coal VM (daf basis) decreased from 16.0% in unaltered coal to 6.9% immediately contact to the sill (Fig. 6b). Accompanying these trends, the ash content (dry basis) increased from 23.6% in unaltered coal sample 10 to 44.6% in heat-affected coal sample 2 (Fig. 6c). The ash content of coal increased towards or near the sill intrusion, as a result of contact-metamorphism. The sill intruded into the No. 10 coal seam through fault and fracture zone especially small cracks during Yanshanian magmatic metamorphism. Moisture decreased from ambient levels of 5.0% to 1.9% in sample 5 and then increased slightly to 3.6% in sample 1 (Fig. 6d). It is possible that the intrusion acted as a seal to prevent moisture loss after magmatic intrusion.

Ultimate analyses showed that the elemental carbon content (daf basis) of coal samples was high and increase slightly toward the sill (Table 1; Fig. 7a). For contact-metamorphism of diorite sill, carbon content increased from 91.2% to 93.9%. The term 'metamorphism' in coal defines a maturation range where at least 90 wt.% of coal is carbon (daf basis) (Schimmelmann et al., 2009). The hydrogen content (daf basis) decreased slightly toward the sill, ranging from 4.5% to 3.5% (Fig. 7b). The oxygen content initially decreased slightly and then increased to a maximum in sample 5, followed by a dramatic decrease and then an increase through sample 1 (Fig. 7c). Nitrogen content with both dry and daf basis initially increased to a maximum in sample 10 and then had decreasing fluctuations toward the sill (Fig. 7d).

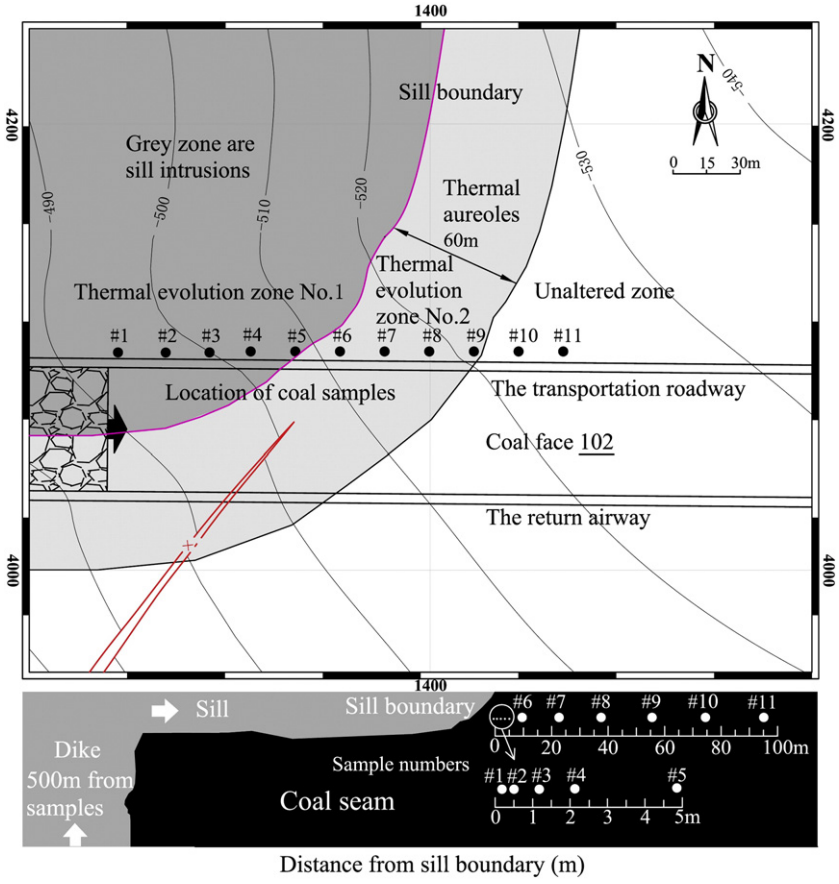

Fig. 4. Planar graph and profile of igneous intrusions and locations of coal samples from Wolonghu Mine. (These isolines are coal-seam floor contour).

The total sulfur distribution in coals around the sill reflects significant contact-metamorphic alteration. In general, total S content in coal is low adjacent to the sill than in more distal coals, while the sample 3 is an exception (Fig. 8). The Wolonghu coal was low in sulfur, with an average total S (dry basis) concentration of 0.25 wt.%, as expressed by the coals that were sampled near the sill. The sample 1 (0.2 m from the sill) adjacent to the sill has the minimum total S value of 0.10 wt.%, sample 2 (0.5 m from the sill) has total S of 0.11 wt.% (Table 1). The atomic ratios N/C, H/C, and O/C experienced decreasing fluctuations approaching the sill from sample 11 to sample 1 (Fig. 9). This could be due to the fluctuations of igneous intrusions.

4.3. Pore size distribution

4.3.1. Surface area

The BET surface areas obtained using low-pressure nitrogen gas adsorption are listed in Table 3.

Table 1
Geochemical and petrographic analyses of Wolonghu coal samples near sill intrusions.

Sample	D (m)	Proximate analysis (wt.%)				Ultimate analysis (wt.%)					Atomic ratios			Macerals (vol.%)			R_o (%)	T (°C)
		Mois	Ash	VM	FC	C	H	O	N	$S_{t,d}$	H/C	O/C	N/C	V	I	M		
#1	0.2	3.6	35.0	6.9	58.4	93.3	3.5	2.6	0.5	0.10	0.449	0.021	0.005	70.8	25.9	3.3	5.03	359
#2	0.5	2.5	44.6	7.9	51.0	93.9	4.0	1.3	0.6	0.11	0.511	0.011	0.0053	70.1	26.0	3.9	4.89	355
#3	1.2	3.2	33.5	9.1	60.6	93.5	4.0	1.4	0.6	0.40	0.511	0.011	0.0052	70.3	26.2	3.5	4.71	350
#4	2.1	3.0	34.2	7.1	67.5	93.2	3.7	0.8	0.9	0.29	0.470	0.007	0.0084	71.0	25.7	3.3	4.82	353
#5	4.8	1.9	40.9	14.5	50.2	91.7	4.4	3.5	0.3	0.09	0.573	0.018	0.0028	71.4	24.7	3.9	4.78	352
#6	9.5	3.6	36.9	12.7	55.1	92.3	4.2	1.9	1.1	0.29	0.551	0.015	0.0104	70.2	26.5	3.3	4.06	331
#7	22.8	3.7	27.7	9.7	65.7	93.3	4.0	1.5	0.8	0.29	0.517	0.012	0.0070	71.4	24.8	3.9	3.67	322
#8	38.7	4.3	36.0	13.6	55.3	91.6	4.7	2.0	1.2	0.28	0.620	0.016	0.0115	73.0	22.0	2.7	3.18	300
#9	56.3	4.2	24.7	12.3	66.1	92.3	4.4	1.8	1.1	0.30	0.574	0.015	0.0103	72.9	23.9	3.2	2.76	282
#10	74.9	3.9	23.6	10.4	68.4	92.1	4.0	2.2	1.4	0.27	0.515	0.018	0.0130	72.9	23.6	3.5	2.75	281
#11	95.1	5.0	33.9	16.0	55.5	91.2	4.5	2.9	0.9	0.36	0.591	0.024	0.0085	74.2	22.1	3.7	2.74	281

D = distance from sill; Mois = moisture; Ash is on a dry basis; VM = volatile matter, on dry ash free (daf) basis; FC = fixed carbon (daf basis); all ultimate analyses reported on a daf basis except sulfur on a dry basis; V = vitrinite, I = inertinite, M = mineral; R_o = random vitrinite reflectance (%, oil); T = estimated paleo temperature (°C) based on Barker and Pawlewicz (1994).

Table 2
Subdivision of maceral composition and max vitrinite reflectance.

Sample	Vitrinite				Inertinite				Minerals			$R_{o,max}$
	Te	Ct	Vi	Ge	Fus	Sf	Ma	In	Cla	Py	Ca	
	(vol.%)				(vol.%)				(vol.%)			(%)
#1	8.7	59.8	0.8	1.5	9.8	8.9	3.5	3.7	2.4	0.5	0.4	5.26
#2	8.5	59.5	0.7	1.4	9.9	7.0	3.9	5.2	2.9	0.4	0.6	5.18
#3	8.7	59.0	0.8	1.8	9.6	5.8	3.9	6.9	2.3	0.4	0.8	4.99
#4	8.1	60.8	0.9	1.2	9.8	5.6	3.6	6.7	2.4	0.4	0.5	4.95
#5	7.8	62.0	0.6	1.0	9.6	5.8	3.7	5.6	3.2	0.3	0.4	4.89
#6	8.2	60.6	0.8	0.6	9.3	6.7	3.6	6.9	3.0	0.2	0.1	4.20
#7	8.1	61.9	0.6	0.8	9.3	6.6	3.5	5.4	3.5	0.3	0.1	3.80
#8	8.9	61.8	1.4	0.9	8.0	5.6	3.5	4.9	2.4	0.3	0	3.28
#9	8.6	62.6	0.9	0.8	8.6	5.9	3.6	5.8	2.9	0.3	0	2.83
#10	8.9	62.2	1.2	0.6	8.8	6.2	3.7	4.9	3.3	0.2	0	2.82
#11	8.4	63.9	1.1	0.8	8.6	5.8	3.4	4.3	3.5	0.2	0	2.83

Te: telinite; Ct: collotelinite; Vi: vitrodetrinite; Ge: gelinite.
Fus: fusinite; Sf: semifusinite; Ma: macrinite; In: inertodetrinite.
Cla: Clay; Py: pyrite; Ca: carbonate. $R_{o,max}$: max vitrinite reflectance (%, oil).

There are large variations in quantities of adsorbed nitrogen among unaltered and heat-affected coal samples (Table 3). The graphs in Fig. 10 demonstrate that the altered coal sample 9 (in thermal evolution zone No. 2) adsorbs largest quantities of nitrogen, the unaltered coal sample 11 (in unaltered zone) adsorbs significantly less nitrogen, and the altered sample 2 (in thermal evolution zone No. 1) from the contact adsorb the least nitrogen (Fig. 10).

These relationships translate directly into BET surface areas calculated from nitrogen adsorption. Sample 9 (56.3 m from sill) had a BET surface area of 22.3 m^2/g, adsorbing the largest quantities of nitrogen. The BET surface area of sample 10, 74.9 m from the sill, was 2.2 m^2/g, which was the lowest value. With decreasing distance to the sill intrusions, the curve of the BET surface area initially increased rapidly and then decreased towards the sill. Samples 5 through 1 closest to the contact (in thermal evolution zone No. 1) show a slightly increasing trend but remains at a low level (Figs. 4 and 11). The thermal evolution of sill intrusions strongly increased the BET surface area of coal samples 6–9, while contact-metamorphism significantly decreased the BET surface area of samples 1–5. However, micropores need to be measured for understanding the underlying causes. The micropores (pores<2 nm) are the main contributors to the total porosity and the surface area. Micropore volume is the primary regulator of high-pressure gas adsorption in the Gates coals (Clarkson and Bustin, 1999).

4.3.2. Micropore characteristics

Micropores obtained using carbon dioxide adsorption are listed in Table 3. The quantity of adsorbed CO_2 increased slightly from unaltered coal samples 11 to 6 with fluctuations, then decreases from sample 6 towards the heat-affected sample 1 (Figs. 12 and 13b).

Plotting micropore surface area and micropore volume against the distance from sill, similar trends are found for both parameters (Fig. 13a, b). With decreasing distance to the sill contact, micropore volumes and micropore surface areas initially increased slightly to maximum in sample 6 (micropore volume = 0.0211 cm^3/g, surface area = 60.5 m^2/g), followed by a dramatic decrease to a minimum in sample 2 (micropore volume = 0.0003 cm^3/g, surface area = 1.2 m^2/g) (Fig. 13a, b). The heat-affected coal (sample 7, R_o = 3.67%) has an average micropore diameter of 1.28 nm, characterizing the highest volumes, whereas the smallest average micropore diameter of 0.71 nm was found in sample 2 (R_o = 4.89%).

Micropore volumes and surface areas closer to the intrusions decreased dramatically, indicating fewer adsorption sites for methane (Mastalerz et al., 2009). The contact-metamorphism dramatically decreased the micropore volume and surface area for sample in the thermal evolution zone No. 1. However, the thermal evolution of sill intrusions in the thermal evolution zone No. 2 plays a slight role in increasing the micropore volume and surface area. More experimental samples are needed to evaluate the effect of the thermal evolution of sill intrusions.

4.4. Adsorption and desorption properties of coal

4.4.1. Gas adsorption properties of coal

Gas is stored in coal mainly by a physical adsorption process. In this process gas is attached to the coal surfaces under a combination of dispersion, repulsion and electrostatic forces. The strength of the adsorption depends on the potential energy of interaction of solid (adsorbent) and gas (adsorbate) which depends on the solid pore system structure and properties of the gas (Saghafi et al., 2008). Five types of adsorption behavior have been found exhibited by various adsorbents and adsorbates (Brunauer et al., 1940). Gregg and Sing (1982) give a detailed description of various isotherm types and their interpretation. One representation of type I isotherm is by the Langmuir model (Langmuir, 1918). The adsorbed gas volumes and gas pressure data are expressed in terms of the Langmuir volume (V_L) and Langmuir pressure (P_L) parameters reported in Table 3. The data are well presented by the Langmuir equation, and the real gas (methane) adsorption isotherms for three represented samples from three zones are seen in Fig. 14.

Sample 2 (0.5 m from sill) in thermal evolution zone No. 1, has a low Langmuir volume of 16.1 m^3/t, Sample 11 (95.1 m from sill) in unaltered zone, has a V_L of 39.1 m^3/t, while sample 8 (38.7 m from sill) in thermal evolution zone No. 2, has a highest V_L of 59.0 m^3/t.

Approaching the sill, the Langmuir volume curve of the eleven samples in three zones initially increased and peaked at V_{Lmax} = 59.0 m^3/t (sample 8) and then decreased rapidly to V_{Lmin} = 13.5 m^3/t (sample 1) (Fig. 15). With contact-metamorphism of diorite sill, the methane adsorption capacity of coal decrease (0–5 m from the sill) in the thermal evolution zone No. 1. However, it increased for the distance 5–60 m from the sill in the thermal evolution zone No. 2 due to the thermal evolution of sill intrusions. This discovery may provide a clue for understanding the mechanism of gas outburst.

4.4.2. Gas desorption properties of coal

Ettinger (1952) was the first one to point out the role of high rates of sorption/desorption of gas in outbursts based on laboratory experiments. The ΔP index (Ettinger et al., 1958), based on the initial rate of gas desorption from coal, has been widely adopted in Europe and elsewhere. Coals with high initial desorption rates are considered prone to instantaneous outbursts (Lidin et al., 1954). In China, the initial gas-releasing rate of coal from soft layer, ΔP is considered one of the four indexes for the identification of coal outbursts. The critical value of ΔP is 10 mm Hg. The ΔP of the eleven coal samples are shown in Table 3.

The ΔP of the coal samples initially increased, reaching a maximum of ΔP_{max} = 40.0 mm Hg (sample 8, in thermal evolution zone No. 2), and then decreased rapidly to 1.3 mm Hg (sample 1) closer to the sill (Fig. 16). Overall, the ability of adsorption and desorption of coal appears in the following sequence: the thermal evolution zone No. 2 > unaltered zone > thermal evolution zone No. 1. The thermal evolution and trap effect of sill and sandstone, making the Wolonghu No. 10 coal seam of the South No. 1 panel (the non-mineable area is ~52%, with thickness of coal<0.3 m) (Fig. 3) more appealing for possible future sequestration of CO_2 from anthropogenic sources.

Interestingly, the BET surface area, micropore volume, ΔP, and L_V curve are positively correlated. The curve of the BET surface area peaks at sample 9, 56.3 m from sill (Fig. 10). Both the micropore volumes and micropore surface areas initially increased slightly to maximum in sample 6, 9.5 m from contact (Fig. 13a,b). Both the L_V and the ΔP index peak at sample 8, 38.7 m from sill (Figs. 15 and 16). All these three samples are in the thermal evolution zone No. 2 (Fig. 4). This observation is validated by the fact that the thermal aureoles of sill is approximately 60 m as previously mentioned. Because of the thermal evolution and

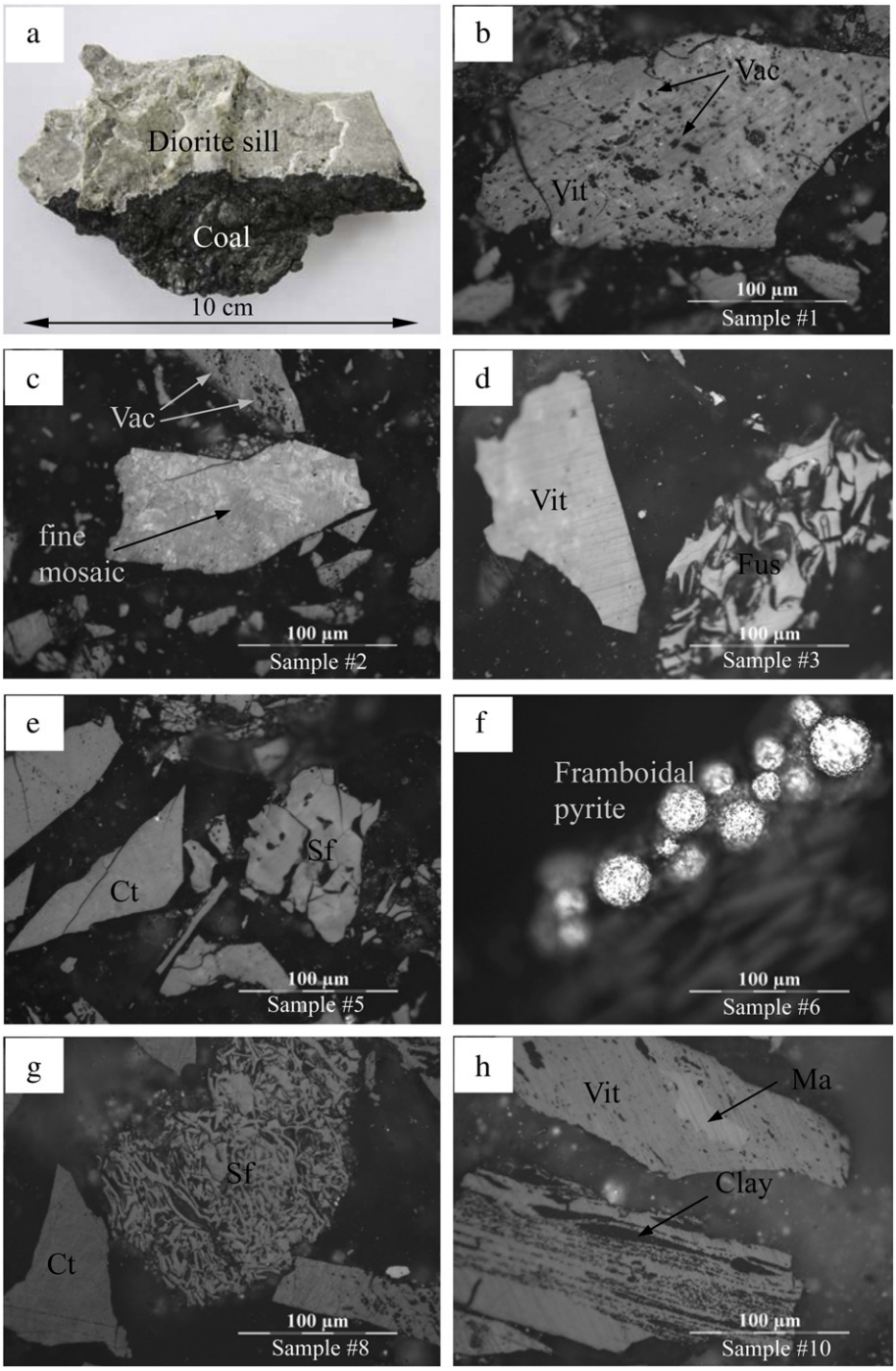

Fig. 5. (a) Megascopic appearance of sill and coal. Photomicrographs b–h of altered and unaltered coal (reflected light, oil immersion 100 μm scale bar). (b) altered vitrinite (Vit) showing devolatilization vacuols (vac), sample 1, $R_o = 5.03$; (c) altered vitrinite (Vit) showing fine mosaic structures and devolatilization vacuols (vac), sample 2, $R_o = 4.89$; (d) vitrinite (Vit) and fusinite (Fus) in altered coal, sample 3, $R_o = 4.71$; (e) altered vitrinite showing Collotelinite (Ct) and semifusinite (Sf) (sample 5), $R_o = 4.78$; (f) Framboidal pyrite enrichment,(sample 6), $R_o = 4.06$; (g) semifusinite (Sf) and Collotelinite (Ct) in altered coal (sample 8), $R_o = 3.18$; (h) vitrinite (Vit), Macrinite of inertinite (Ma) and Clay in the form of veins (Cla) in unaltered coal (sample 10), $R_o = 2.75$.

trap effect of sill intrusion, the abnormally high formation pressure was created, and two outbursts occurred in the No. 10 coal seam due to the effect of sill trapping.

4.5. Effects of sill intrusions on the generation and retention of methane

4.5.1. Abnormally high formation pressure

Extensive gas pressure data were acquired during the extension and preparation of the No. 10 coal seam. Fig. 17 shows the relationship between the pressure and the elevation relative to sea level. The gas pressure values of measuring point beneath −450 m (below the sea level) all greater than the critical value of outburst, 0.74 MPa, according to China's national standard (State Administration of Coal Mine Safety of China, 2009b). The biggest pressure observed was 4.4 MPa at coalface 104, not far from one of the locations of coal and gas outburst (Fig. 3).

The underground gas pressures obtained in the No. 10 coal seam can be described by linear regressions above (Eq. (2)) and below (Eq. (3)) an elevation of −450 m:

$$P = -0.003 \times H - 0.158 \quad (2)$$

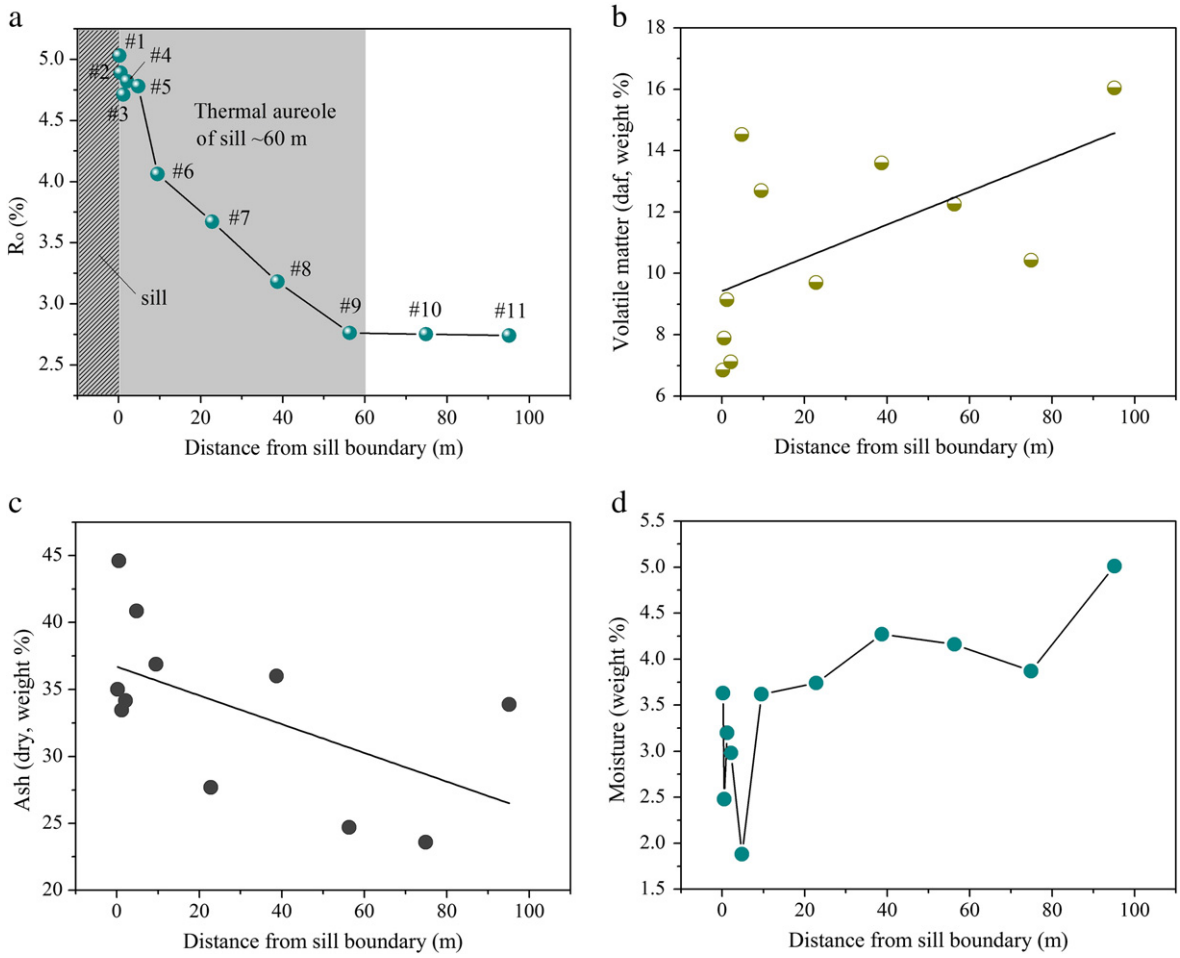

Fig. 6. Relationships between distance from sill boundary and vitrinite reflectance (a), volatile matter (b), ash yield (c), and moisture content (d).

$$P = -0.027 \times H - 11.322 \quad (3)$$

where P is the gas pressure in MPa and H is the elevation of the coal seam in m. The gas pressure gradient (slope of a linear regressions shown in Fig. 17, in MPa/m) of No. 10 coal seam at an elevation above −450 m was 0.003 MPa/m. However, the gradient of elevation below −450 m was 0.027 MPa/m, higher than normal hydrostatic pressure 0.01 MPa/m. This is usually called abnormally high formation pressure (AHFP) (Polutranko, 1998; Su et al., 2005). Two causes are believed to form the abnormally high pressure in the Wolonghu No. 10 coal seam. Firstly, in the normal region, most of the roof and floor are sandstone and mudstone, which have a good tightness effect. With the addition of trap effect of the sills and dikes in the igneous intrusion zone, a sealing reservoir could be formed. Secondly, the coal has a stronger methane adsorption and storage capacity close to the sill intrusion zone, which plays a decisive role to form the abnormally high pressure.

4.5.2. Gas content

The gas contents of the No. 10 coal seam at coalface 108 above −450 m are shown in Table 4. In situ gas contents were determined according to the formula (4):

$$T = D + L + R_1 + R_2 \quad (4)$$

where T is the total in situ gas contents (m^3/t), D is the desorption gas content in the mine (m^3/t), L is the gas loss content (m^3/t), R_1 is the negative pressure desorption gas content before comminution (m^3/t), R_2 is the negative pressure desorption gas content during comminution (m^3/t). L was obtained from the empirical formula, while R_1 and R_2 were determined in the laboratory. Gas volume was converted to standard conditions.

Despite few data points, an increasing trend with depth in the gas content of No. 10 coal can be seen. The coalbed gas content was 12.3 m^3/t at an elevation of −360 m and 22.7 m^3/t at −381 m. Higher gas content should be expected below −450 m.

The trap effect of the igneous intrusion is closely related to the abnormally high formation pressure in the No. 10 coal seam. The No. 10 coal seam is an inclined seam with an inclination of 10° towards southwest. It was formed by a bottom-up invasion on a ring by magma in the Yanshanian magmatic metamorphism. After a long geology period, coal bed methane above −450 m was released in part through the oxidation of the coal outcrop (Fig. 3). The gas content dropped along the gas pressure gradient. For below −450 m, the thermal evolution of magmatic igneous rock is believed to made micropores develop and increase both methane adsorptive capacity and gas content.

4.6. Implications for outbursts

The coal seams in the Wolonghu Mine were very rich in methane, with an absolute emission of 56.7 m^3/min and a relative emission of 70.0 m^3/t. A permanent extraction system for methane was built, and the extracted methane is used to generate electricity. However,

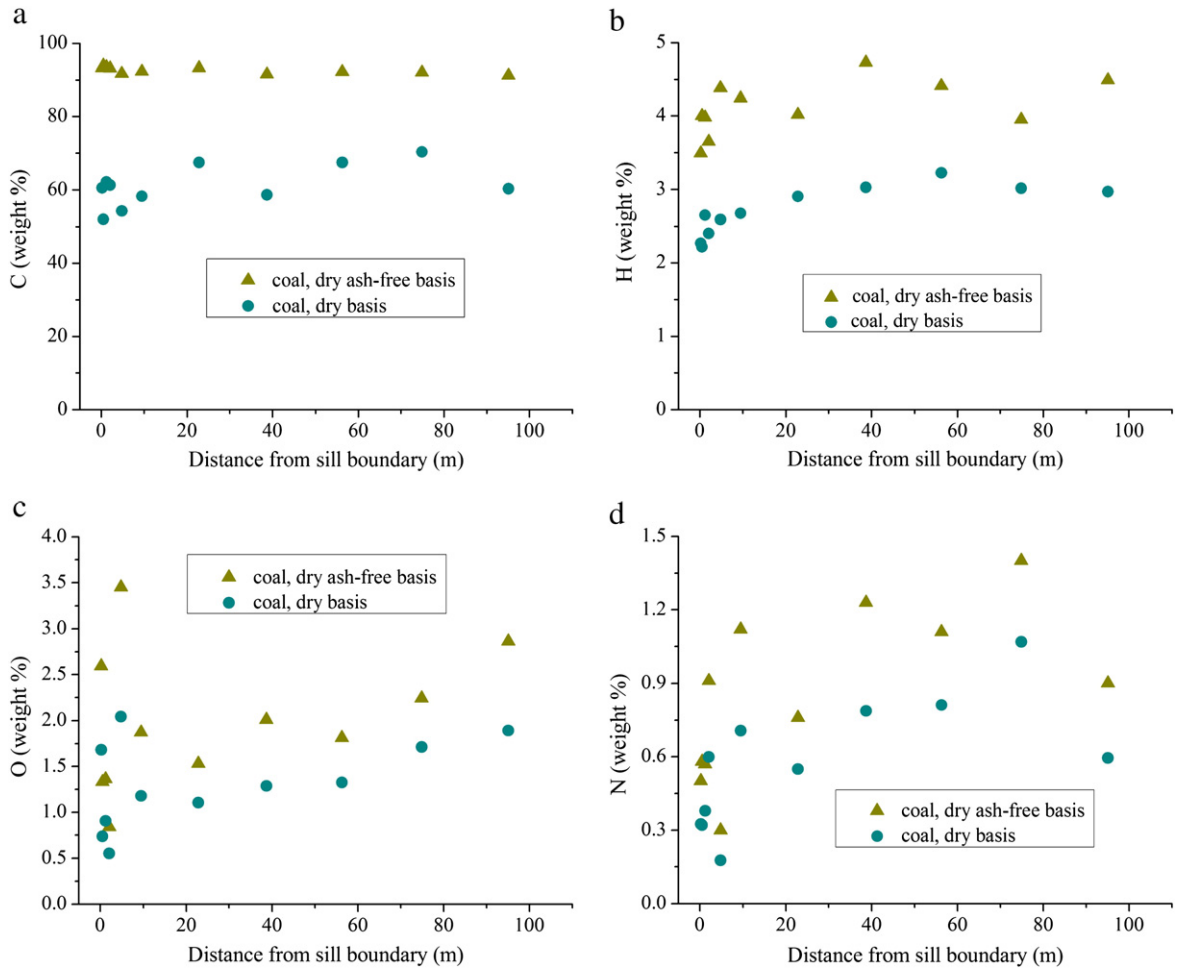

Fig. 7. Relationship between distances from sill and carbon (a), hydrogen (b), oxygen (c), and nitrogen (d) content.

there have been two outbursts in No. 10 coal seam since the mine was built (Fig. 3). The first outburst occurred on January 6, 2006 in the airway of coalface 101 in the No. 10 coal seam. The outburst occurred at −555 m (below the sea level). Thirty-seven tons of coal and 10,000 m^3 of methane were ejected. The second outburst occurred on August 12, 2008, in the transportation roadway of coalface 105 in the same coal seam at a level of −429 m. A total of 29.5 t and 3361.2 m^3 of coal and methane, respectively, were released. The outburst distance reached 7.9 m.

The locations of the outbursts were 8 m and 38 m from the sill boundary, and they occurred in the thermal evolution zone No. 2 (Fig. 3). The sill acted as an impermeable barrier, the trap effect is a result of the sill along the roof and dike from the fault belt forms of the No. 10 coal seam. The mudstone and siltstone roof and floor of

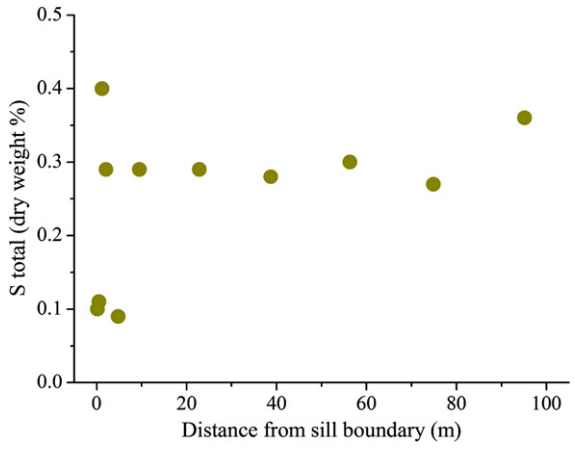

Fig. 8. Relationship between distances from sill and total sulfur content.

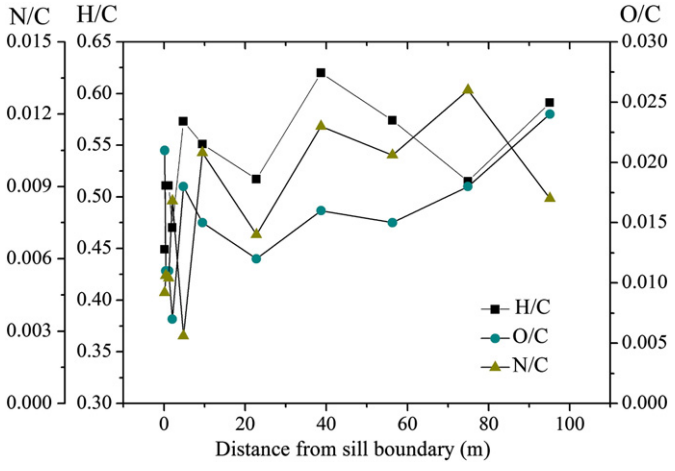

Fig. 9. Relationship between distances from sill and atomic ratios N/C, H/C, and O/C.

Table 3
Pore characteristics, adsorptive capacity and methane initial desorption rates of coal samples.

Sample	Units	#1	#2	#3	#4	#5	#6	#7	#8	#9	#10	#11
Distance from sill	m	0.2	0.5	1.2	2.1	4.8	9.5	22.8	38.7	56.3	74.9	95.1
BET surface area	m^2/g	4.3	3.3	3.5	3.1	1.9	16.1	10.3	15.0	22.3	2.2	6.5
D-R micr. surface area	m^2/g	4.6	1.2	1.4	6.2	1.9	60.5	58.6	56.3	58.3	51.6	54.8
D-A micropore volume	cm^3/g	0.0008	0.0003	0.0005	0.0052	0.0004	0.0211	0.0204	0.0196	0.0203	0.0179	0.0185
Avg. micropore size	nm	1.05	0.71	0.86	1.16	0.73	1.25	1.28	1.22	1.23	1.23	1.24
V_L	m^3/t	13.5	16.1	28.1	36.0	26.3	56.5	45.7	59.0	52.0	47.1	39.1
P_L	kPa	4570	5112	8230	1070	10,650	624	659	638	721	731	483
ΔP	mm Hg	2.3	1.6	1.3	3.0	11.0	30.8	32.8	40.0	38.6	30.0	31.0

Micropore (pores<2 nm); V_L = Langmuir volume; P_L = Langmuir pressure; ΔP = initial gas-releasing rate.

the normal zone have a better sealing. Thus both the effects form gas pockets and lead to abnormally high formation pressure and occurrences of two outbursts (Figs. 3 and 17).

Based on the range of the thermal aureoles of magma, methane control zoning method should occur at least 60 m from the sill, and local prevention measures should be strengthened in the thermal evolution zone No. 2 (Fig. 4). In addition, the gas drainage pressure should be higher, and the drainage time should be increased. Excavatory activity must occur under safe procedures after eliminating the local risk of an outburst. Understanding of relationship between methane outburst and sill intrusions and outburst mechanism, however, requires further rigorous research.

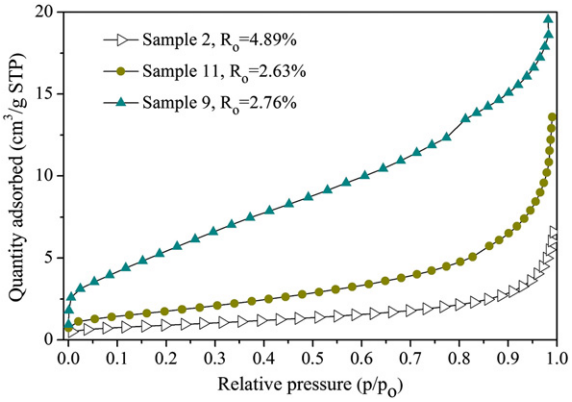

Fig.10. Quantities of nitrogen gas adsorbed onto coal at relative pressure. Note that significantly less nitrogen is adsorbed onto heat-affected coal sample 2 and unaltered coal sample 11 compared to coal sample 9 in thermal evolution zone No. 2.

5. Conclusion

No. 10 coal comes from the Wolonghu Mine of the Permian-age Huaibei Coalfield, located in the north of Anhui Province in China. This anthracite C coal has been affected by igneous intrusion. Thermal alteration of the sill was ~60 m, forming three zones. Approaching the sill, values of R_o increased from ~2.74% to ~5.03%, forming devolatilization vacuoles and fine mosaic texture. VM (daf) decreased from 16.0% to 6.9%. Moisture decreased from 5.0% to 1.9% and then increased to 3.6%, and %C (daf) ranged from 91.2% to 93.9%, %H (daf) from 4.7% to 3.5%, %N (daf) from 1.4% to 0.5%, and total S (dry) from 0.36 wt.% to 0.10 wt.% at the sill boundary. Gradients are lager near the intrusions, although the data fluctuates.

Contact-metamorphism dramatically decreased the methane adsorption capacity of coal (0–5 m from the sill), while thermal evolution of sill strongly increased it (5–60 m from the sill).With decreasing distance to the intrusions, the Langmuir volume curve of the eleven samples initially increased and peaked at V_{Lmax} = 59.0 m^3/t (sample 8) and then decreased rapidly to V_{Lmin} = 13.5 m^3/t (sample 1). The BET surface areas and ΔP index of the coal samples in the thermal evolution zone No. 2 were greater than in the two other zones, and the unaltered zone had higher values than the thermal evolution zone No. 1. This discovery could provide a clue for understanding the mechanism of gas outburst. The sill acted as an impermeable barrier. The trap effect of sill, in conjunction with the mudstone and siltstone roof and floor of the normal zone, sealed the No. 10 coal seam, forming a gas pocket. There has been an

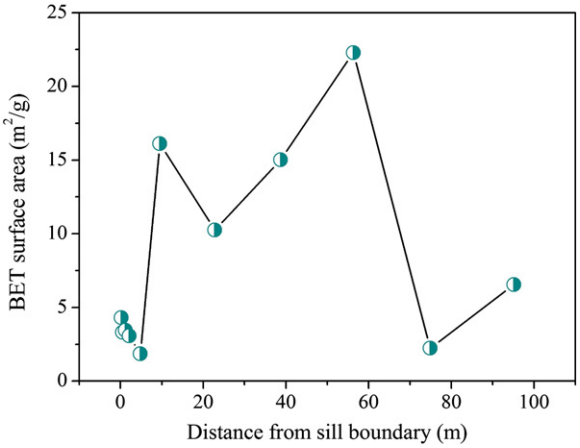

Fig. 11. Relationship between BET surface area and distance from sill boundary.

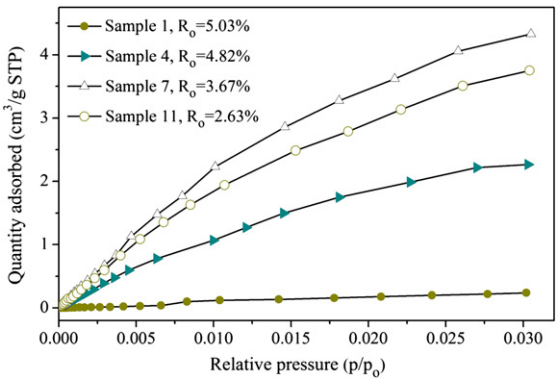

Fig. 12. Quantities of carbon dioxide adsorbed onto coals at relative pressure. Note that significantly less CO_2 is adsorbed onto samples 1 and 4 near the intrusive contact compared to samples 7 and 11 at larger distances from sill.

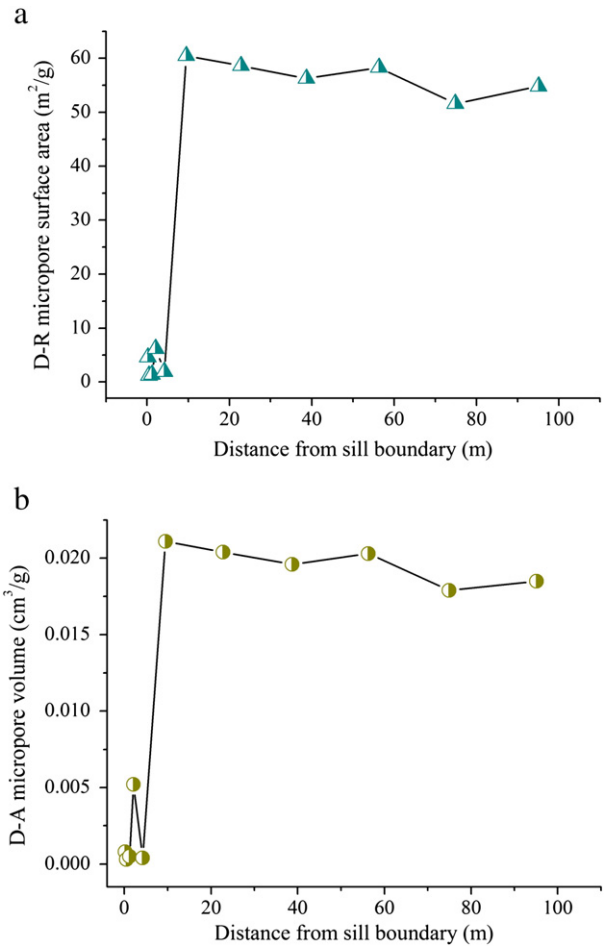

Fig. 13. Evolution of micropore surface area and micropore volume with decreasing distance from sill (a, b).

abnormally high pressure formation and two gas outbursts due to the effects of sill trapping.

Acknowledgments

The authors are grateful to senior engineer Yanjun Liu from the Wolonghu Mine of Hengyuan Coal Electricity Group Co., Ltd., for their assistance with first-hand information on the coalfield. The authors acknowledge Professors Shifeng Dai and Qixiang Yu of CUMT for their valuable comments. Funding for this research was provided by the National Basic Research Program of China (973 Program, No. 2011CB201204) and the National Foundation for the Youth of China (No. 51004106).

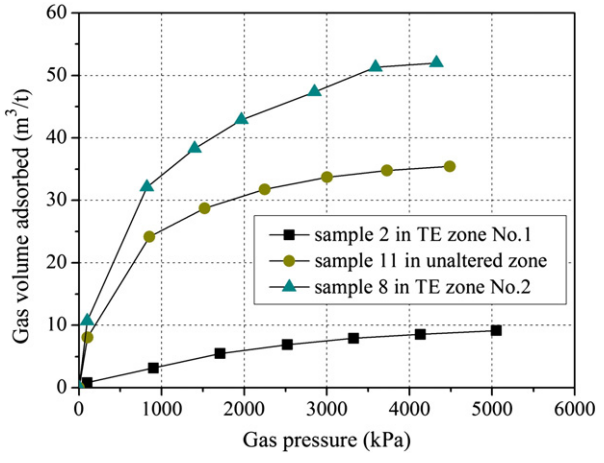

Fig. 14. Comparison of gas (methane) adsorption behavior of three samples, sample 2 (0.5 m from sill) in thermal evolution (TE) zone No. 1, sample 8 (38.7 m from sill) in TE zone No. 2, sample 11 (95.1 m from sill) in unaltered zone.

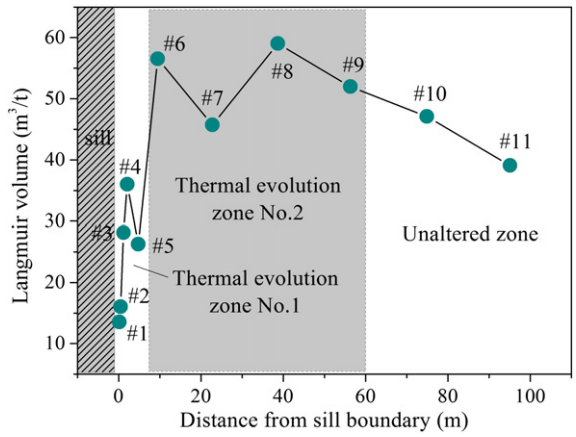

Fig. 15. Relationship between Langmuir volumes of samples in three zones and distance from sill.

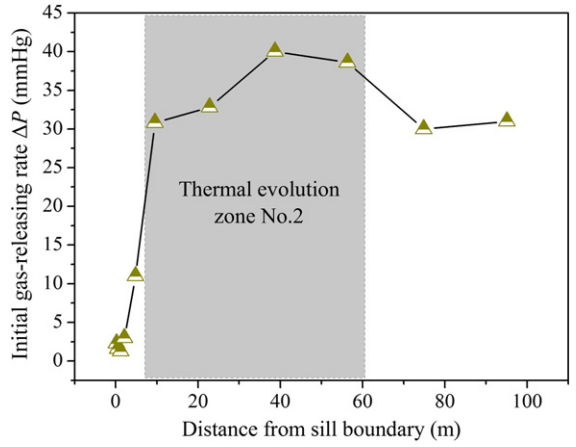

Fig. 16. Relationship between initial gas-releasing rate and distance from sill.

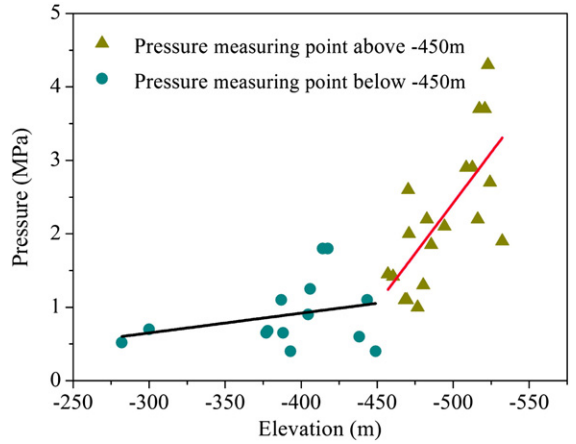

Fig. 17. Relationship between gas pressures of No. 10 coal seam and elevation in ring-sill trap zone.

Table 4
Gas contents of No. 10 coal seam above −450 m.

Location of coal samples	Elevation (m)	L (m^3/t)	D (m^3/t)	R_1 (m^3/t)	R_2 (m^3/t)	T (m^3/t)
Coalface 108 roadway	−360	1.5	0.3	8.7	1.8	12.3
Coalface 108 roadway	−365	2.1	0.6	8.9	1.9	13.5
Coalface 108 roadway	−371	4.3	1.6	9.5	2.1	17.5
Coalface 108 roadway	−381	6.3	1.7	10.1	4.6	22.7

T = total gas contents; D = desorption gas content in mine; L = loss gas content; R_1 = the negative pressure desorption gas content before comminution; R_2 = desorption gas content during comminution.

References

Anderson, S.B., 1995. Outbursts of methane gas and associated mining problems experienced at Twistdraai Colliery. In: Lama, R. (Ed.), Proceedings of the Int. Symposium Cum Workshop on Management & Control of High Gas Emissions & Outbursts, Wollongong, pp. 423–434.

ASTM, 2007. Annual Book of ASTMStandards. Section Five, Petroleum Products, Lubricants, and Fossil Fuels, vol. 05.06. ASTM International, West Conshohocken, PA. 711 pp.

Barker, C.E., Pawlewicz, M.J., 1994. In: Mukhopadhyay, P.K., Dow, W.G. (Eds.), Calculation of vitrinite reflectance from thermal histories and peak temperatures: a comparison of methods: Vitrinite Reflectance as a Maturity Parameter: Amer. Chem. Soc. Symp. Ser., 570, pp. 216–229.

Beamish, B.B., Crosdale, P.J., 1998. Instantaneous outbursts in underground coal mines: an overview and association with coal type. International Journal of Coal Geology 35, 27–55.

Brunauer, S., Deming, L.S., Deming, E., Teller, J., 1940. On a theory of the van der Waals adsorption of gases. American Chemical Society 62, 1723–1732.

Clarkson, C.R., Bustin, R.M., 1999. The effect of pore structure and gas pressure upon the transport properties of coal: a laboratory and modeling study. 1. Isotherms and pore volume distributions. Fuel 78, 1333–1344.

Clegg, K.E., 1955. Metamorphism of coal by peridotite dikes in southern Illinois: Ill. St. Geol. Surv. Rept. Invest., 178, pp. 17–18.

Cooper, J., Crelling, J., Rimmer, S., Whittington, A., 2007. Coal metamorphism by igneous intrusion in the Raton Basin, CO and NM: implications for generation of volatiles. International Journal of Coal Geology 71, 15–27.

Dai, S.F., Ren, D.Y., 2007. Effects of magmatic intrusion on mineralogy and geochemistry of coals from the Fengfeng–Handan coalfield, Hebei, China. Energy & Fuels 21, 1663–1673.

Dai, S.F., Zou, J.H., Jiang, Y.F., Ward, C.R., Wang, X.B., Li, T., Xue, W.F., Liu, S.D., Tian, H.M., Sun, X.H., Zhou, D., 2011. Mineralogical and geochemical compositions of the Pennsylvanian coal in the Adaohai Mine, Daqingshan Coalfield, Inner Mongolia, China: modes of occurrence and origin of diaspore, gorceixite, and ammonian illite. International Journal of Coal Geology. doi:10.1016/j.coal.2011.06.010.

Dutcher, R.R., Campbell, D.L., Thornton, C.P., 1966. In: Given, P.H. (Ed.), Coal metamorphism and igneous intrusives in Colorado: Coal Science: Amer. hem. Soc. Advances in Chemistry Series, vol. 55, pp. 708–723.

Ettinger, I.L., 1952. PokazateI sklonnosti ugla k vybrosam ugla i gaza. Ugol 10, 31–34.

Ettinger, I.L., Zhupakhina, E.S., Schterenberg, L.E., 1958. Methods of Allowing Forecasting in the Seams of Coal Zoned Subject to Instantaneous Outbursts. Extract from Academy of Sciences of the USSR, Institute of Mines Central Committee of Measures Against Instantaneous Outbursts, Moscow, Cherchar Translation No. 111–50, Paris.

Faiz, M.M., Saghafi, A., Barclay, S.A., Stalker, L., Sherwood, N.R., Whitford, D.J., 2007. Evaluating geological sequestration of CO_2 in bituminous coals: the southern Sydney Basin, Australia as a natural analogue. International Journal of Greenhouse Gas Control 1, 223–235.

Golab, A., 2004. Changes in geochemistry and mineralogy of thermally altered coal, Upper Hunter Valley, Australia. International Journal of Coal Geology 57, 197–210.

Golab, A., Carr, P., Palamara, D., 2006. Influence of localised igneous activity on cleat dawsonite formation in Late Permian coal measures, Upper Hunter Valley, Australia. International Journal of Coal Geology 66, 296–304.

Gregg, S.J., Sing, K.S.W., 1982. Adsorption, Surface Area and Porosity. Academic Press, New York.

Gurba, L.W., Weber, C.R., 2001. Effects of igneous intrusions on coalbed methane potential, Gunnedah Basin, Australia. International Journal of Coal Geology 46, 113–131.

Han, S.F., 1990. Coal-forming geological conditions and forecast of Huainan and Huaibei coal region. Geology press, Beijing, pp. 8–118.

ISO 7404–5, 1984. Methods for the Petrographic Analysis of Bituminous Coal and Anthracite—Part 5: Method of Determining Microscopically the Reflectance of Vitrinite. 11 pp.

Jiang, B., Qu, Z., Wang, G.G.X., Li, M., 2010. Effects of structural deformation on formation of coalbed methane reservoirs in Huaibei coalfield, China. International Journal of Coal Geology 82, 175–183.

Langmuir, I., 1918. The adsorption of gases on plane surfaces of glass, mica and platinum. Journal of the American Chemical Society 40, 1361.

Li, W., Cheng, Y.P., Wang, L., 2011. The origin and formation of CO_2 gas pools in the coal seam of the Yaojie coalfield in China. International Journal of Coal Geology 85, 227–236.

Lidin, D.L., Ettinger, I.L., Zhupakhina, E.S., Sazonov, L.V., 1954. Determination of the rate of gas emission as a method of detecting zones liable to sudden outbursts. Ugol 29, 21–24.

Liu, D.M., Yao, Y.B., Tang, D.Z., Tang, S.H., Yao, C., Huang, W.H., 2009. Coal reservoir characteristics and coalbed methane resource assessment in Huainan and Huaibei coalfields, Southern North China. International Journal of Coal Geology 79, 97–112.

Mastalerz, M., Drobniak, A., Schimmelmann, A., 2009. Changes in optical properties, chemistry, and micropore and mesopore characteristics of bituminous coal at the contact with dikes in the Illinois Basin. International Journal of Coal Geology 77, 310–319.

Polutranko, A., 1998. Causes of formation and distribution of abnormally high formation pressure in petroleum basins of Ukraine: Abnormal Pressures in Hydrocarbon Environments, 70, pp. 181–194.

Pross, J., Pletsch, T., Shillington, D.J., Ligouis, B., Schellenberg, F., Kus, J., 2007. Thermal alteration of terrestrial palynomorphs in mid-Cretaceous organic-rich mudstones intruded by an igneous sill (Newfoundland Margin, ODP Hole 1276A). International Journal of Coal Geology 70, 277–291.

Rimmer, S.M., Yoksoulian, L.E., Hower, J.C., 2009. Anatomy of an intruded coal, I: effect of contact metamorphism on whole-coal geochemistry, Springfield (No. 5) (Pennsylvanian) coal, Illinois Basin. International Journal of Coal Geology 79, 74–82.

Sachsenhofer, R.F., Privalov, V.A., Panova, E.A., 2011. Basin evolution and coal geology of the Donets Basin (Ukraine, Russia): an overview. International Journal of Coal Geology. doi:10.1016/j.coal.2011.05.002.

Saghafi, A., Pinetown, K., Grobler, P., Vanheerden, J., 2008. CO_2 storage potential of South African coals and gas entrapment enhancement due to igneous intrusions. International Journal of Coal Geology 73, 74–87.

Sarana, S., Kar, R., 2011. Effect of igneous intrusive on coal microconstituents: study from an Indian Gondwana coalfield. International Journal of Coal Geology 85, 161–167.

Schimmelmann, A., Mastalerz, M., Gao, L., Sauer, P.E., Topalov, K., 2009. Dike intrusions into bituminous coal, Illinois Basin: H, C, N, O isotopic responses to rapid and brief heating. Geochimica et Cosmochimica Acta 73, 6264–6281.

Stach, E., Mackowsky, M.-T.h., Teichmiiller, M., Taylor, G.H., Chandra, D., Teichmiiller, R., 1982. Coal Petrology. Bomtraeger, Stuttgart. 535 pp.

State Administration of Coal Mine Safety of China, 2007. The Direct Measuring Method of the Coal Seam Gas Pressure in Mine.

State Administration of Coal Mine Safety of China, 2008. The Direct Method of Determining Coalbed Gas Content in the mine.

State Administration of Coal Mine Safety of China, 2009a. Determination Method for Index (ΔP) of Initial Velocity of Diffusion of Coal Gas.

State Administration of Coal Mine Safety of China, 2009b. Provisions of the Prevention of Coal and Gas Outburst.

Stewart, A., Massey, M., Padgett, P., Rimmer, S., Hower, J., 2005. Influence of a basic intrusion on the vitrinite reflectance and chemistry of the Springfield (No. 5) coal, Harrisburg, Illinois. International Journal of Coal Geology 63, 58–67.

Su, X., Lin, X., Liu, S., Zhao, M., Song, Y., 2005. Geology of coalbed methane reservoirs in the Southeast Qinshui Basin of China. International Journal of Coal Geology 62, 197–210.

Taylor, G.H., Teichmüller, M., Davis, A., Diessel, C.F.K., Littke, R., Robert, P., 1998. Organic Petrology. Gebrüder Borntraeger, Berlin. 704 pp.

Valentim, B., Guedes, A., Rodrigues, S., Flores, D., 2011. Case study of igneous intrusion effects on coal nitrogen functionalities. International Journal of Coal Geology 86, 291–294.

Yang, M., Liu, G.J., Sun, R.Y., Chou, C.L., Zheng, L.G., 2011. Characterization of intrusive rocks and REE geochemistry of coals from the Zhuji Coal Mine, Huainan Coalfield, Anhui, China. International Journal of Coal Geology. doi:10.1016/j.coal.2011.06.012.

Zhang, W.Y., Xu, S.P., Cai, X.B., 2005. Magmatic intrusion of the Wolonghu Mine and its Effect on coal seams, coal quality, methane. Geology of Anhui 15, 25–28.

Zheng, L.G., Liu, G.J., Qi, C.C., Zhang, Y., Wong, M.H., 2008. The use of sequential extraction to determine the distribution and modes of occurrence of mercury in Permian Huaibei coal, Anhui Province, China. International Journal of Coal Geology 73, 139–155.